

An MRI study on the disentangling of a nest-like column of long rods under vertical shaking

Jing Yang¹, Yuwen Sun¹, and Chengjie Xia^{1,*}

¹Shanghai Key Laboratory of Magnetic Resonance, School of Physics and Electronic Science, East China Normal University, Shanghai, China

Abstract. Highly anisotropic granular particles can form very loose and stable piles with a large repose angle due to the geometric cohesion effect. The random geometric features of such structures and the origin of their stability against external mechanical perturbations remain to be explored. Here, using magnetic resonance imaging techniques, we perform an accurate structural reconstruction of columns built with long granular rods. We study the structural evolution during the gradual disentangling and collapse of a randomly poured free-standing pile of long rods under consecutive vertical shaking. The average height of the column decreases exponentially upon shaking, accompanied by a nonmonotonic evolution of the average packing fraction and an increasing negative nematic order of the rod orientations. Yet, the distributions of the relative position and orientation of contacting rod pairs remain roughly unchanged during the disentangling process. Distribution and spatial correlation between contact points as well as the evolution of contact network have also been analysed, providing insights into the micromechanics of nest-like structures.

1 Introduction

Packings of grains with highly anisotropic or nonconvex shapes can exhibit exceptional mechanical strength due to geometric cohesion [1], though the underlying mechanism remains unclear. Such randomly-assembled, strong structures can be found in both natural and artificial systems, for example, in bird nests or concrete tetrapods used for coastal protection [2]. While the mechanical rigidity for spherical granular packings may be linked to a hard-sphere glass [3], extending these theories to highly non-spherical systems remains challenging [4].

The global mechanical behaviours of various non-convex granular packings have been extensively studied, with particular focus on how particle shape influences mechanical and structural properties [5-8]. Recent work has also explored the micromechanical origin of plasticity in random rod packings [9]. An alternative approach to understanding the mechanical stability of a granular column involves analysing its collapse under external perturbations and the associated agitation and relaxation dynamics [10]. For instance, in U-shaped granular materials, stability appears to arise from a competition between packing fraction and the number of entangled structures [11], although exact contact-scale mechanism remains unclear. Moreover, for convex objects such as the long rod studied here, it is still poorly understood how entanglement and geometric cohesion emerge in such systems.

In this study, we investigate the collapse and disentanglement process of long rod columns subjected to vertical shaking. Using magnetic resonance imaging

(MRI) combined with image processing techniques, we first reconstruct the three-dimensional packing structures. We then present preliminary analyses of contact point distributions and contact network geometries, revealing distinct structural features related to the system's mechanical behaviour.

2 Methods

2.1 Experiments

Each granular rod is a hollow 3D-printed plastic cylinder filled with water to enable the magnetic resonance imaging. The rods have a length $L_0 = 100$ mm and a diameter $D_0 = 4$ mm. In the experiment, about 600 rods were randomly poured into a cylindrical container (20 cm in diameter), forming a column of approximately 18 cm in height (Fig. 1(a)). The container, which is open at the bottom, was then gently lifted and removed without disturbing the column. The free-standing column remained stable on the underpan without lateral support from the container walls. After acquiring MRI scans of the column's initial state using a medical MRI scanner (MAGNETOM Prisma Fit, Siemens Healthcare, Erlangen, Germany), the entire column was lifted by 1 cm via a pulley system attached to the underpan and then released to impact the scanner bed. The collision generated vibrations, causing partial disentanglement and collapse of the column. We refer this process as one shaking event. *In situ* scanning of the structure was repeated after 1, 4, 9, 16, 25, 36, 51, 71

* Corresponding author: cjxia@phy.ecnu.edu.cn

and 101 shaking events. Fifteen independent experimental trials were conducted.

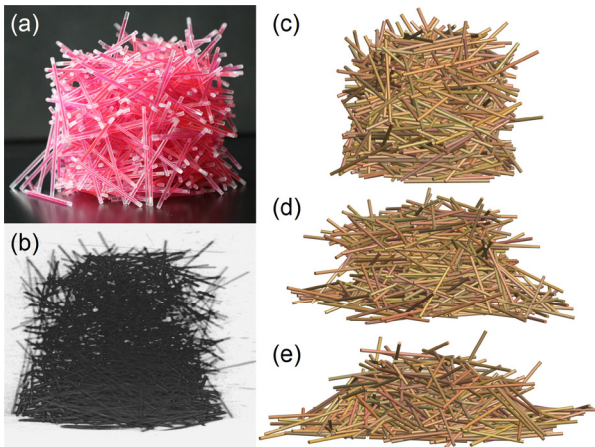


Fig. 1. (a) Photograph of the free-standing granular rod column. (b) A 3D magnetic resonance image showing water voxel distribution within all rods. (c-e) Reconstructed column structures after 0 (c), 16 (d) and 51 (e) times of shaking.

2.2 Image processing and reconstruction

We applied a super-resolution algorithm to the raw MRI data (Fig. 1(a)), enhancing the spatial resolution from the original 0.8 mm/pixel by a factor of three. Because only the water inside the rods generates strong magnetic resonance signals, individual rods appear distinctly separated in the images. This enables a straightforward identification of each rod's voxels, allowing direct calculation of both centroid positions and orientation vectors. This approach has been tested in our previous studies of granular disks [12].

To minimize artificial rod overlaps caused by imaging artifacts, we use a Monte Carlo optimization procedure [13]. In this approach, each rod's position and orientation undergo small stochastic perturbations around their initial values. A perturbation is accepted only if it reduces the total overlapping volume between rods. This refinement process improves the reconstruction accuracy. The uncertainty of rod centroid is about $0.3D_0$ along the rod's orientation and $0.1D_0$ in perpendicular directions. The error in rod orientation is about 0.8° . Meanwhile, we generalize the error-function fitting method for the tomographic images of granular spheres to identify contacts between rods [14]. Three reconstructed packing structures at different stages of collapse are shown in Fig. 1(c-e).

2.3 Definition of packing fraction

The packing fraction of a granular packing is conventionally defined as the ratio of the total particle volume to the packing volume. However, this definition becomes ambiguous for free-standing columns without clear boundaries. To address this issue, we develop the following method to calculate the characteristic packing fraction in such systems. First, we discretize each rod by selecting $L_0/D_0 = 25$ evenly spaced points along its cylindrical axis. For each point, we identify an optimal plane that maximizes the number of rod points on one

side. The normal vector of this plane approximates the local density gradient of the system. We then define $p \leq 1$ as ratio of the number of points on either side of the plane, where $p \approx 0$ indicates proximity to the column periphery and $p \approx 0.5$ corresponds to central regions. Finally, we obtain a convex hull bounded by all planes with $p < p_t$, compute the total rod volume within this hull, and determine the corresponding packing fraction $\Phi(p_t)$. Naturally, Φ increases monotonically with p_t . When p_t exceeds a critical threshold $p^* \approx 0.07$, $\Phi(p_t)$ plateaus, allowing us to define $\Phi = \Phi(p^*)$ as the characteristic packing fraction of the system. We have verified that p^* remains roughly unchanged for different packings.

3 Results

3.1 Column collapse process

Fig. 2(a) shows that the centroid height of a column, defined as the average vertical distance between rod centroids and the base, decreases exponentially with shaking time, consistent with observations in U-shaped granular packings [11]. This exponential decay persists across columns with diameters ranging from about 17 to 30 cm with the same number of rods, though thinner columns typically fracture in the middle after several shaking cycles. During the collapse, we observe that rods closer to the vertical direction are more likely to slide down. To quantify this orientational dependence, we use a nematic order parameter $S_z = \langle 3(\mathbf{n} \cdot \hat{\mathbf{z}})^2 - 1 \rangle / 2$, where \mathbf{n} is the unit orientation vector of each rod, $\hat{\mathbf{z}}$ is the vertical unit vector, and $\langle \circ \rangle$ denotes an average over all rods in the column. As shown in Fig. 2(b), negative S_z values indicate preferential horizontal alignment due to gravity. Also, S_z decreases approximately logarithmically with shaking time during the initial collapse stage.

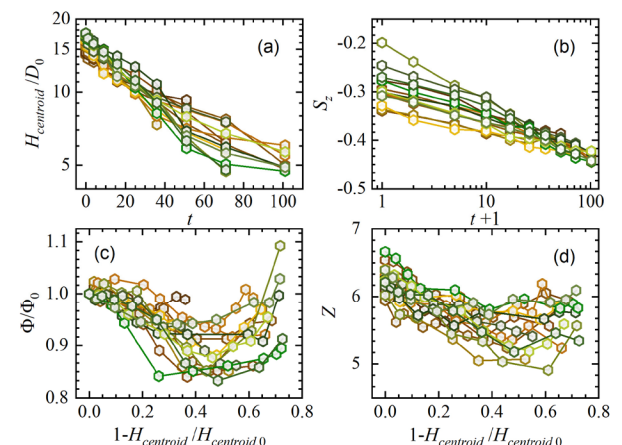


Fig. 2. (a) Temporal evolution of the column's centroid height $H_{centroid}$ and (b) nematic order parameter versus shaking time t . (c, d) The relationships between average packing fraction Φ (c), average contact number Z (d) and $H_{centroid} \cdot \Phi$ and $H_{centroid}$ are normalized by their initial values: Φ_0 and $H_{centroid,0}$. Different symbols represent different realizations of the experiment.

Unexpectedly, the average packing fraction shows a nonmonotonic relationship with the centroid height (Fig.

2(c)). The averaged initial packing fraction is about 0.22, and it decreases by about 10% upon shaking and increases at the final stage of the collapse. The average contact number exhibits the same nonmonotonic trend. At the early stage of the collapse, the stronger negative nematic order for looser packings is consistent with our recent results on very short granular spherocylinders [15], highlighting a common mechanical origin of this orientational ordering. Yet, the final densification of the column represents a different regime. It is similar to a shaking-induced compaction of grains confined in a container, except that the remaining structures of the column at the end of collapse is self-supporting.

3.2 Contact point distribution

To investigate how geometric features influence mechanical stability of the columns, we analyse contact point distributions on individual rods. Each rod is described in a local coordinate system (Fig. 3(a)), where \hat{z}' is a unit vector along the rod's axis, oriented to form an acute angle with \hat{z} , \hat{x}' is parallel to the cross product $\hat{z}' \times \hat{z}$, and $\hat{y}' = \hat{x}' \times \hat{z}'$. The origin is fixed at the rod's centroid. Contact positions are parameterized using cylindrical coordinates (θ_c, z_c) , representing azimuthal and height coordinates respectively.

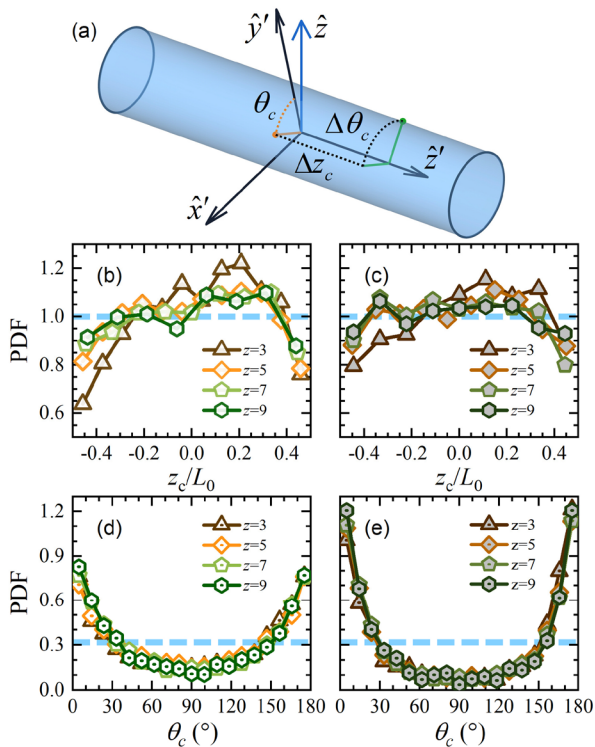


Fig. 3. (a) Local coordinate system definition for a rod. (b, c) Height z_c and (d, e) azimuthal angle θ_c probability distribution functions (PDFs) of contact points, comparing initial state (b, d) and those after 51 times of shaking (c, e). Different symbols represent rods with different number of contacts, and dashed lines represent uniform distributions.

The contact point distribution is nonuniform. The contact points cluster away from the rod ends and display a slight bias towards the upper half, that is: $\langle z_c \rangle > 0$ (Fig. 3(b, c)). These axial preferences weaken both for rods with more contacts and during later collapse stages. In contrast, a much stronger angular

preference can be noticed, with contacts predominantly located on the top and bottom surfaces, that is, θ_c close to 0° and 180° (Fig. 3(d, e)). This orientational order persists regardless of the contact number but intensifies with stronger collapse level, that is, a larger S_z . These observations clearly demonstrate how contact geometry stabilizes the column against gravitational forces.

Furthermore, we observe a nontrivial correlation between contact points on individual rods. For each pair of contact points on one rod, we calculate their axial separation Δz_c and azimuthal difference $\Delta \theta_c$. By binning the data by Δz_c and averaging $\Delta \theta_c$ within each bin, we find that contact pairs with $\Delta z_c < 0.5L_0$ preferentially occupy opposite rod surfaces, that is, with $\Delta \theta_c > \pi/2$, while those with larger axial separations tend to cluster on the same side (Fig. 4). We attribute this anti-correlation at small separations to torque balance constraints governing individual rod stability.

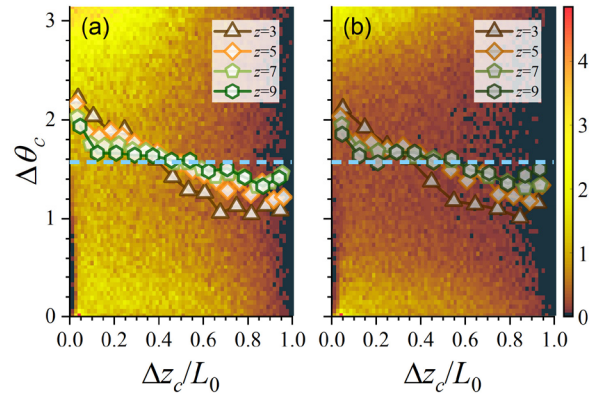


Fig. 4. Average azimuthal distance $\Delta \theta_c$ as a function of height difference Δz_c of contact points on a rod, for (a) the initial packings, and (b) those after 51 times of shaking. Different symbols represent rods with different number of contacts. The dashed lines represent $\Delta \theta_c = \pi/2$, indicating uniform angular distribution. Background colour maps represent the joint probability distribution of $(\Delta z_c, \Delta \theta_c)$.

3.3 Contact loops

To elucidate how contact geometry governs the column's mechanical strength, we analyse contact loops, in which several rods contacting with one another consecutively and form a closed loop. For each rod in a loop of n rods, (which we referred as an n -loop), we define the edge length l_n as the axial separation Δz_c between its two contact points connecting adjacent rods. A loop is considered entangled when all constituent rods exhibit angular separations $\Delta \theta_c > \pi/2$ of their individual pairs of contact points with other rods in the loop. These entangled loops impose mutual constraints on rod mobility, as illustrated in Fig. 5(c, d).

To investigate whether contacting rods exhibit spatial correlation in loop formation, we generate randomly distributed contact points uniformly along the rods and calculate the PDFs of the length of n edges that can form a closed n -loop. Comparing experimental PDFs with these uncorrelated distributions reveals that 3-loops are noticeably shorter than the random case, while 4-loops are close to the uncorrelated distributions (Fig. 5(a, b)). Loops composing more than four rods

show qualitatively similar behaviours to those of the 4-loops.

Furthermore, we find that entangled n -loops have longer average edge length compared to their unentangled counterparts (Fig. 5(e, f)). During column collapse, 3-loops show a gradual increase in edge length, with entangled loops expanding at a slightly higher rate. While 4-loops initially follow this trend, their average edge length undergoes rapid shortening after about 30 times of shaking. This transition point coincides with both the minimal packing fraction and contact number preceding the late-stage re-compaction of the column. These observations show that the column collapse is accompanied with a gradual disentangling of contact loops, with entangled 3-loops displaying particular stability. This suggests that such 3-loop configurations may serve as fundamental structural units providing stability to the column.

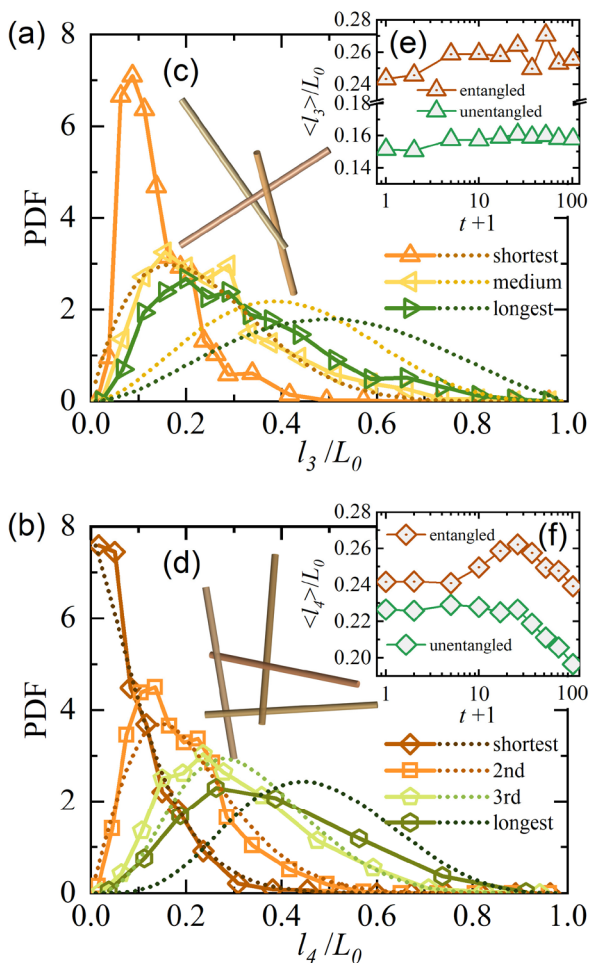


Fig. 5. (a, b) PDFs of edge length of contact loops. Different symbols represent edges lengths in a sequential order. The dotted lines represent uncorrelated cases with uniform contact point distributions. (c, d) Examples of entangled loops. (e, f) Average edge lengths of entangled (symbols with a dot at centre) and unentangled loops (open symbols). Data and pictures are show for 3-loops (a, c, e) and 4-loops (b, d, f).

4 Conclusion

In this work, we study the collapse process of a column of long granular rods under vertical shaking. The MRI and image processing techniques allow us to reconstruct

the packing structures with a relatively high accuracy. During the collapse, the average packing fraction and contact number evolve nonmonotonically, suggesting a two-stage structural evolution: the disentangling of relatively unstable structures at the beginning of the collapse, followed by a compaction of the remaining stable structures. The orientational orders of rods and contact points, as well as the spatial correlations of contact positions coherently suggest that the mechanical stability requirement leaves evident geometric features in the column structure, and thus, there could exist some hidden intrinsic structures (such as the entangled contact loops) that play the role of a rigid backbone of the system.

This work was supported by the Natural Science Foundation of Shanghai (Grant No. 24ZR1419900). The authors would also like to thank Bingwen Hu and Jianqi Li for project coordination.

References

1. S. V. Franklin, *Physics Today* **65**, 70 (2012).
2. N. Weiner, Y. Bhosale, M. Gazzola, and H. King, *J. Appl. Phys.* **127**, 050902 (2020).
3. Y. Xing, Y. Yuan, H. Yuan, S. Zhang, Z. Zeng, X. Zheng, C. Xia, and Y. Wang, *Nat. Phys.* **20**, 646 (2024).
4. T. Borzsonyi and R. Stannarius, *Soft Matter* **9**, 7401 (2013).
5. K. A. Murphy, N. Reiser, D. Choksy, C. E. Singer, and H. M. Jaeger, *Granular Matter* **18**, 26 (2016).
6. Y. C. Zhao, K. Liu, M. Zheng, J. Barés, K. Dierichs, A. Menges, and R. P. Behringer, *Granular Matter* **18**, 24 (2016).
7. L. Y. Meng, C. Wang, and X. H. Yao, *Physica A* **490**, 212 (2018).
8. W. Deng, L. F. Liu, Y. Yuan, and S. X. Li, *Powder Technol.* **383**, 443 (2021).
9. Y. Bhosale, N. Weiner, A. Butler, S. H. Kim, M. Gazzola, and H. King, *Phys. Rev. Lett.* **128**, 198003 (2022).
10. M. Trepanier and S. V. Franklin, *Phys. Rev. E* **82**, 011308 (2010).
11. N. Gravish, S. V. Franklin, D. L. Hu, and D. I. Goldman, *Phys. Rev. Lett.* **108**, 208001 (2012).
12. Y. Ding, J. Yang, C. Wang, Z. Wang, J. Li, B. Hu, and C. Xia, *Phys. Rev. Lett.* **131**, 098202 (2023).
13. G. W. Delaney, T. Di Matteo, and T. Aste, *Soft Matter* **6**, 2992 (2010).
14. T. Aste, M. Saadatfar, and T. J. Senden, *Phys. Rev. E* **71**, 061302 (2005).
15. Y. W. Sun, C. Y. Wang, J. Yang, W. J. Shi, Q. F. Pang, Y. J. Wang, J. Q. Li, B. W. Hu, and C. J. Xia, *Phys. Rev. E* **110**, 014903 (2024).